

Stall, spiculate or runaway - the fate of fibers growing towards fluctuating membranes

D. R. Daniels¹, D. Marenduzzo², M. S. Turner¹

¹ Department of Physics, University of Warwick, Coventry CV4 7AL, UK

² SUPA, School of Physics, University of Edinburgh, Mayfield Road, Edinburgh EH9 3JZ, UK

We solve the dynamic equations of motion for a growing semi-flexible polymer, or fiber, approaching a fluctuating membrane at an angle. At late times we find three different regimes: fiber *stalling*, when fiber growth stops due to membrane resistance, *run-away*, in which the polymer bends away from the membrane, and another regime in which the membrane response is nonlinear and tubular membrane *spicules* are formed. We discuss which regions of the resulting ‘phase diagram’ are explored by (i) single and bundled actin fibers in living cells, (ii) sickle hemoglobin fibers in red blood cells, and (iii) microtubules growing within artificial vesicles. We complement our analysis with full 3-dimensional stochastic simulations.

PACS numbers: 87.16.Ka, 82.35.Lr, 36.20.Ey, 87.16.Dg

Semi-flexible polymer fibers, making up the cytoskeleton, interact with fluctuating membranes continuously in living cells [1]. The polymerisation of filaments such as actin, with persistence lengths $l_p \sim 10\mu\text{m}$, can deform the outer plasma membrane of the cell, giving rise to protrusions that can be sheet-like (lamellipodia) or more localised (filopodia) [1]. Forces are thought to arise through polymerisation at the fiber tips [2, 3]. A similar mechanism is thought to drive growth of sickle hemoglobin fibers, leading to a pathological rigidification of red blood cells [4], as well as microtubules, such as can be grown in artificial vesicles [5].

While the phenomenon of Euler buckling of a fiber of fixed length impinging on a solid obstacle at an angle is well studied (see e.g. [6] and Refs. therein), the case in which the elastic fiber is growing, and the obstacle is a fluctuating membrane, have so far received much less attention, despite its more direct relevance to biological systems. Thus here we propose a set of equations of motion that describe the coupled dynamics of a growing semi-flexible polymer close to a fluctuating membrane (Fig 1). We complement this treatment with full 3-dimensional dynamic Monte-Carlo (3dMC) simulations. Our main focus is on the dynamic regimes attained at late times. We find that fibers may (i) *stall*, (ii) *run-away*, i.e. bend away from the membrane, or (iii) cause the formation of tubular membrane *spicules*. What differentiates our approach from earlier work is the explicit description of the flexibility of both the membrane and the polymer [3, 6, 7, 8, 9], which allows us to include all three fates of the fiber.

The Hamiltonians governing the membrane and the polymer elasticity, respectively H_m and H_p , are given by :

$$H_m = \frac{1}{2} \int d^2r \left(\kappa_m (\nabla_\perp^2 u)^2 + \sigma (\nabla_\perp u)^2 \right) \quad (1)$$

$$H_p = \frac{\kappa}{2} \int_0^L ds \left(\frac{\partial \theta}{\partial s} \right)^2$$

where κ_m and σ denote the membrane rigidity and surface tension respectively and are typically $\kappa_m \sim 10^{-19} \text{ J}$ and $\sigma \sim 10^{-4} \text{ Jm}^{-2}$ for biomembranes, u measures the normal deviation of the membrane from local flatness, which we take to be the plane $z = 0$, $\kappa = k_B T l_p \equiv l_p / \beta$ is the polymer

bending rigidity, L is its (instantaneous) length and $\theta(s, t)$ is the angle between the local direction of the fiber at arc length position s and the plane $z = 0$ at time t , see Fig 1. Our use of an explicit Hamiltonian to describe the flexibility of both the membrane and polymer differentiates our approach from earlier work [3, 6, 7, 8, 9]. The probability distribution of the membrane displacement can be calculated from the conditional partition function that it is at fixed height z_m at one point. This is here approximated by [10] $\mathcal{Z}_m = \exp(-A z_m^2)$, where $A = \frac{2\pi\sigma}{\log\left(1 + \frac{\sigma\Omega}{\kappa_m\pi^2}\right)}$, Ω being the area of the ‘frame’

supporting the membrane patch under consideration. A measures the membrane ‘softness’ ($A \rightarrow \infty$ corresponds to a hard wall), and typically $A \sim 10^{-4} \text{ Jm}^{-2}$ [10]. The partition function \mathcal{Z}_m can be integrated over all allowed z_m to obtain the normal force acting on the fiber tip due simply to the steric repulsion between tip and membrane. As is common in studies of buckling we perform a saddle point approximation on H_p in Eq. 1, and consider the adiabatic limit in which, at all times, the fiber is in equilibrium. This is reasonable in all physical cases as the fiber relaxation time (at most ms) is much smaller than the inverse polymerisation rate (typically 0.01-1 s). We seek to solve the following coupled equations for the fiber shape, growth rate and tip height and the normal force on the tip, respectively

$$0 = \left[\kappa \frac{\partial^2 \theta(s, t)}{\partial s^2} - f \cos(\theta(s, t)) \right] \quad (2)$$

$$\frac{\partial L(t)}{\partial t} = \delta \left\{ k_{\text{on}} e^{[-\beta f(\Delta) \delta \sin(\theta(L(t), t))]} - k_{\text{off}} \right\} \quad (3)$$

$$\Delta(t) = -d + \int_0^{L(t)} ds \sin(\theta(s, t)) \quad (4)$$

$$f(\Delta) = 2\sqrt{\frac{A}{\pi}} \frac{\exp(-A(\Delta(t))^2)}{1 - \text{erf}(\sqrt{A}\Delta(t))} \quad (5)$$

Here $k_{\text{on}, \text{off}}$ are, respectively, the rates of polymerisation and depolymerisation at the fiber tip, d and Δ the initial and instantaneous distances between the fiber tip and the membrane frame, δ the increase in length upon addition of a monomer, while $f(\Delta)$ is the force exerted by the membrane on the fiber

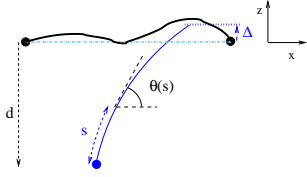


FIG. 1: Sketch of the system under consideration. A growing fiber is obliquely incident onto a fluctuating membrane, which is anchored to some distant frame. The fiber is clamped at $s = 0$ and its length at time t is $L(t)$.

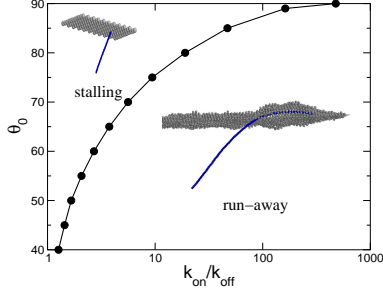


FIG. 2: Plot of the critical angle θ_c (solid line) below which a run-away transition occurs, as a function of k_{on}/k_{off} , for actin-like parameters ($d = 100$ nm, $\kappa = 10 k_B T \mu m$, $\sqrt{A}\delta \sim 0.8$, $\delta = 2.5$ nm). (The run-away state shown on the right is obtained with 3dMC simulations with $\theta_0 = 45^\circ$, $k_{on}/k_{off} = \infty$ and $\sqrt{A}\delta = 0.4$.)

tip [10]. We assume constant rates $k_{on,off}$ but time varying rates could be included to model, e.g. actin concentration fluctuations. The fiber is treated as if clamped at one end $\theta(s=0, t) \equiv \theta(s=0) \equiv \theta_0$, into the cytoskeletal mesh, while the end at $s = L(t)$ is free, $(\partial\theta(s, t)/\partial s)_{s=L(t)} = 0$. Eq. 5 has been derived by assuming that the membrane and the fiber only interact via excluded volume and that this can be introduced at a single point (the fiber tip) [10]. This may fail for a highly bent fiber that often contacts the membrane far from its tip [11]. We solve Eqs. 2-4 numerically, via a standard Euler relaxation algorithm and finite difference discretisation. The solutions for the system of Eqs. 2-5 fall into two classes. The fiber can either (a) grow until it stalls, or (b) undergo a run-away transition [8]. This is distinct from usual fiber buckling, which is a purely equilibrium phenomenon. The physical parameters determining the system dynamics are the four dimensionless quantities $\sqrt{\frac{A}{k_B T}}\delta$, k_{on}/k_{off} , $\frac{\kappa\delta}{k_B T d^2}$, and d/δ . Eq. 2 neglects fluctuations around the average fiber shape (see below for a discussion of the effect of these). Throughout we work at physiological temperature T .

Fig. 2 shows a cut of the ‘phase diagram’: for $\theta_0 > \theta_c$ the fiber ultimately stalls, otherwise it is bent away by the membrane. Here θ_c is established by variation of k_{on}/k_{off} , for parameters typical of actin fibers in cells (see caption).

As the incidence angle approaches the critical threshold from below, the growth of the fiber is strongly non-linear at intermediate times (see Fig. 3a). This is because the growth rate is reduced by a factor exponential in $f(\Delta)$ (see Eq. (2)).

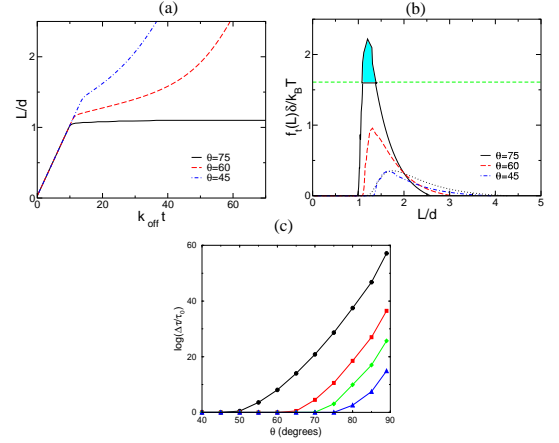


FIG. 3: For three different initial incidence angle θ_0 we show (a) the fiber length as a function of time, and (b) the tangential adiabatic force f_t as a function of length. Here $k_{on}/k_{off} = 5$ (other parameters as Fig. 2), so that the stalling force is $\log(5)k_B T/\delta$, and the fiber is stalled for $\theta_0 = 75^\circ$ and runs away at the two smaller incidence angles. This diagram serves to show that *all* stalled states are metastable. The analytical prediction for the adiabatic longitudinal force (dotted line) is compared to the numerical result for $\theta_0 = 45^\circ$. The time needed to tunnel the barrier to run-away growth can be estimated as being proportional to the exponential of an energy barrier, being the area of the coloured region for $\theta_0 = 75^\circ$ in (b). The linear-logarithmic plot of this tunneling time as a function of its initial incidence angle, found by an application of Kramers’ theory, is shown in (c). From top to bottom, $k_{on}/k_{off} = 1.1, 1.5, 3, 5$ and 10 .

This force bends the tip (Eq. (1)) and as a result the growth speeds up again, as the factor $\sin(\theta(L(t), t))$ decreases (Eq. (2)). Far from the transition line this behaviour is not found and the fiber growth is nearly linear at all times, see Fig. 3a.

The physics of the transition between the metastable stalled state and the run-away state is controlled by the *tangential* force on the fiber tip $f_t(L)$, see Fig. 3b – f_t is related to the normal force in Eq. 5 via a factor $\sin(\theta(L))$ to be determined self consistently from Eqs. 2-5. If the thermodynamic stall force $f_{stall} = (k_B T/\delta) \log(k_{on}/k_{off})$ is above the maximum of f_t the fiber runs away, otherwise the fiber stalls when it reaches the length at which the membrane generated force equals its thermodynamic stalling force. However, as the adiabatic force vanishes for very long fibers, the stalled state is, in fact, metastable and the fiber may still run away provided it can ‘tunnel’ through the free energy barrier present. Using elementary transition state theory, we can estimate the time required for such a tunneling event as $\Delta\tau = \tau_0 \exp\left(\int_{L_1}^{L_2} dL f_t\right)$ where $\tau_0 \sim$ ms is a typical microscopic relaxation time (or inverse attempt frequency) and L_1 and L_2 are given by intercepts of the force curve with the thermodynamic stall force, see Fig. 3b. Fig. 3c shows a representative plot of $\Delta\tau$ versus θ_0 , with actin-like parameters.

Actin fibers in cells can be biochemically capped [1]. If the tunneling time is larger than the inverse capping rate, typically < 1 s, the fiber growth will be halted. Tunneling from the

metastable stalled state may thus often be negligible.

While Eqs. 2-5 have to be solved numerically, one can employ a Gaussian approximation for the fiber tip fluctuations, controlled by H_p in (1), which permits some analytic analysis and, in particular, yields an explicit formula for $f_t(L)$.

To achieve this, starting from Eq. 1, we adopt a standard path integral method [10], and compute the first two moments of the probability distribution for the fiber tip position

$$\langle z_p \rangle_0 = 2\kappa \sin \theta_0 \left(1 - \exp \left(-\frac{L}{2\kappa} \right) \right) \quad (6)$$

$$\langle z_p^2 \rangle_0 = 4\kappa^2 \left(\frac{L}{2\kappa} + \exp \left(-\frac{L}{2\kappa} \right) - 1 - \frac{\cos 2\theta_0}{12} \right. \\ \left. \left(3 + \exp \left(-\frac{2L}{\kappa} \right) - 4 \exp \left(-\frac{L}{2\kappa} \right) \right) \right) \quad (7)$$

where the subscript 0 denotes the fact that these are derived in the absence of a membrane. Using these moments we can approximate the distribution of heights z_p of the tip of the semiflexible polymer by a Gaussian distribution, $\mathcal{Z}_p = \exp \left(-B(z_p - \langle z_p \rangle_0)^2 \right)$ where $B = \frac{1}{2} \frac{1}{\langle z_p^2 \rangle_0 - \langle z_p \rangle_0^2}$. This approach is appropriate provided the force on the fiber is \ll the Euler buckling threshold, $\pi^2 \kappa / (4L^2)$. So far we have calculated *separately*: (i) the membrane deformation, and (ii) the fiber tip distributions. We now introduce the steric *interaction* between the rod and membrane as follows:

$$\mathcal{Z}_{tot} = \int_{-\infty}^{\infty} dz_m \int_{-\infty}^{\infty} dz_p \mathcal{U}(z_m - z_p) \mathcal{Z}_m \mathcal{Z}_p \\ = \frac{1}{2} \left(1 - \operatorname{erf} \left(\frac{\langle z_p \rangle_0 - d}{\sqrt{1/A + 1/B}} \right) \right) \quad (8)$$

where $\mathcal{U}(x) = 1$ if $x > 0$ and 0 otherwise.

It is reassuring that for completely rigid fibers we recover the corresponding result derived in Ref. [10]. Using \mathcal{Z}_{tot} one can calculate, e.g. the tangential force acting on the tip $f_L = -\frac{\partial \log(\mathcal{Z}_{tot})}{\partial L}$. This can be directly compared with the full numerical treatment (see Fig. 3b, in which the comparison is shown for a fiber with $\theta_0 = 45^\circ$). For small incidence angle, up to $\theta_0 \approx 55^\circ$ (with the parameter values of Figs. 2-3), the agreement is good, breaking down gradually as the initial incidence angle approaches normal incidence. The smoother force rise in the analytics for $\theta_0 = 55^\circ$ is due to the inclusion of tip fluctuations, which do not alter the value of the maximum. (We note that if the membrane is floppier than the agreement persists to a larger angle.) To see why the analytics eventually break down, we note that invoking a Gaussian tip distribution amounts to replacing the fiber with a spring with a Hookean constant B , which becomes stiffer with θ_0 . For θ not too close to 90° , $B \simeq \frac{3\kappa}{2L^3 \cos^2(\theta)}$, in agreement with the treatment of Ref. [6]. Our combined treatment of fiber tip and membrane fluctuations using a Gaussian distribution can be seen as the natural generalisation of the elastic fiber model of Refs. [3, 6] to the case of a fluctuating soft membrane. As the incidence angle becomes close to normal, intuition suggests that the tip fluctuations will become ‘one-sided’ and the Gaussian approximation may then become poor.

We note from Fig. 2 that in an eukaryotic cell (where $k_{on}/k_{off} \sim 100$ [3]), $\theta_c \sim 86^\circ$ for an actin fiber. Thus the majority of fibers in a cytoskeletal actin network may be expected to eventually run away from the membrane. Fibers stall at smaller angles than this if the initial fiber-membrane separation is smaller (than $d = 100$ nm). Electron microscopy of the actin network [12] reveals that some of the fibers *do* appear to be bent into a sub-membrane ‘thatchwork’, which may help the cytoskeleton sustain stress although might contribute less efficiently to motility. However in lamellipodia and filopodia, observed at the leading edge of a moving cell, the fibres are actively pushing with their tips pointing towards the membrane [13]. It is then natural to ask what ‘countermeasures’ a moving cell takes to avoid run away.

One efficient strategy is to combine many fibers into a thicker, thus stiffer, bundle. If n fibers are cross-linked into one bundle, e.g. by the Ena/VASP proteins or the ‘tip complex’ [13], the aggregate can still be described as a single fiber obeying Eqs. 2-5, up to a rescaling $\delta \rightarrow \frac{\delta}{n}$, $k_{on,off} \rightarrow n k_{on,off}$ and $\kappa \rightarrow n^2 \kappa$, which amounts to assuming that the fibers are strongly cross-linked. As a result of bundling both stalling and run-away occur at larger membrane forces.

Fig. 4 shows how the dynamic ‘phase diagram’ of Fig. 2 gets modified by bundling. Here we have taken $n = 10$, which may be a reasonable assumption for small filopodia *in vivo* [7]. Solving Eqs. 2-5 shows that θ_c decreases with n , so that the stalling regime widens (Fig. 4). More importantly, a stiffer fiber, or a bundle with larger n , will deform the membrane more. As a result if n is large enough, and θ_0 is close to 90° , non-linear membrane deformation into tubular spicules [9] may occur before run-away. We adopt a rough test for when spicules will be formed that is related to the breakdown of the linear membrane Hamiltonian (1), specifically that the maximum average membrane gradient exceeds unity $\langle |\nabla_\perp u|_{max} \rangle > 1$. It can be shown [10] that this spiculation condition can be translated to a condition on the average membrane displacement, namely that it exceeds $\langle z_m \rangle = d + \frac{1}{2A} \frac{\partial \log(\mathcal{Z}_{tot})}{\partial d}$, which can be calculated from (8) $\langle z_m \rangle - d = \frac{5\pi}{2A} \sqrt{\kappa_m \sigma}$. Inserting appropriate physical values we estimate that spicules form only if the (maximum) membrane displacement is at least ~ 100 nm or, equivalently, that the normal membrane force is ~ 80 pN [14]. Note that the boundary between spicule formation and fiber run-away is not sensitive to the polymerisation rate, unlike the boundary between spicule formation and stalling. Thus, for physiological parameters, there is only a finite range of incidence angle for which a bundled actin fiber can form a filopodium.

We know of at least two other mechanisms beyond fiber bundling which the cell may employ to avoid excessive run-away of actin fibers: (i) capping proteins [1], (ii) tethering of fiber tips to the membrane [6].

It is also interesting to consider a series of *in vitro* experiments aimed at controlling cell motility via protein expression [15] in lights of our results. These experiments showed that lamellipodia only form when capping proteins are present in the cell, so that they can be thought of as a dense network

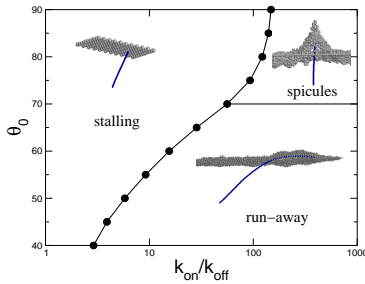


FIG. 4: Phase diagram for a bundle of $n = 10$ actin fibers, with parameters obtained by scaling those used for Fig. 2 to this bundle size (see text). The insets are 3dMC simulations obtained with parameter values as in Fig 2 except the spicule for which $\sqrt{A}\delta = 0.1$.

of short and mostly artificially stalled fibers. Depleting the cell of capping proteins, without decreasing the amount of Ena/VASP proteins, results in massive growth of filopodia, akin to spicules. Reducing the number of Ena/VASP proteins as well, leads on the other hand to the formation of membrane ruffles, which may be associated with extensive fiber run-away, in agreement with what we predict for actin fibers polymerising with cell-like conditions. All the states in our phase diagram can thus be obtained in a cell by regulating the concentrations of these key proteins.

The validity of our treatment is not limited to single and bundles actin fibers. Microtubules and sickle hemoglobin fibers may have parameters closer to $\delta \sim 0.5$ nm and $\kappa \sim 0.1 - 1$ mm. If we adopt $d \sim 1$ μ m, comparable to the size of the cell, stalling occupies a smaller region in the dynamic ‘phase diagram’, and run-away and spicule formation a larger region. This is in agreement with experiments [5].

Nonlinear membrane deformations, leading to spicule (or filopodia) formation cannot be described quantitatively using Eqs. 2-5. To check our approximate analytical threshold for the onset of spicule formation, we have performed full 3-dimensional Monte-Carlo dynamic simulations, in which both membrane and fiber are discretised into connected ‘beads’. A time step in the dynamic evolution consists of attempting to move the position of all beads in both the fiber and the membrane via local moves (see Refs. [8, 16] for details on the algorithm). A local move is accepted according to the Metropolis test with discretised versions of Eq. 1.

Examples of run-away state and spicule, found via our simulations, are shown as insets in Figs. 2 and 4. (Parameters are given in the legends.) For $\theta_0 = 90^\circ$, we confirm that there is a crossover between run-away and spiculation. For $\sqrt{A}\delta \simeq 0.2$ this occurs when the persistence length of the polymers exceeds $1.5 - 2$ μ m, in good agreement with 1.25 μ m found using our Gaussian approximation. In few cases for lower l_p values the fiber does not run away, but is ‘trapped’ by the membrane fluctuations giving rise to a spicule. We also find that the run-away state (see Figs. 2 and 4) gives rise to a bump in the membrane which may account for the observation of ruffles [15]. Finally, if we require that a fiber does not run-away for 10^8 Monte-Carlo steps, 3dMC simulations pre-

dict that the crossover to the run-away state in Fig. 1 occurs for $\theta_c \simeq 85^\circ$ for $k_{\text{on}}/k_{\text{off}} = 100$, which is in good agreement with $\theta_c \simeq 86^\circ$ found via Eqs. 2-5.

In conclusion, we have solved the dynamic equations of motion for a growing semi-flexible polymer, incident onto a fluctuating soft membrane at an angle, and found a dynamic transition between fiber run-away and stalling. Given the kinetic polymerisation rate of actin fibers in the cell, we predict that single actin fibers should bend and run away from the membrane, and would not contribute to cell motility. This is in agreement with *in vitro* investigations under unphysiological conditions in which the behaviour of cells lacking bundling and capping proteins was investigated. Moving cells seems to have taken ‘precautions’ to stop this phenomenon from happening excessively, by bundling or capping fibers to render them stiffer. Our phase diagram can be generalised to the case of an actin bundle, and we show that in this case a third regime appears, in which the fiber deforms the membrane in a non-linear fashion and spicules appear, which are akin to the filopodial protrusions observed in motile cells. It is intriguing that physiological values of the thermodynamic parameter $\log k_{\text{on}}/k_{\text{off}}$ can be seen to lie in, or close to, the narrow range of values for which actin filopodia can explore all three different destinies. Finally, we predict that microtubules and sickle hemoglobin fibers should be more likely to form spicules or to run away than to stall, in agreement with observations.

This work was supported by NIH (NHLBI) grant HL58512 and EPSRC grant GR/S29256/01.

-
- [1] D. Bray, *Cell movements: from molecules to motility*, 2nd edition, Garland Publishing (2001); B. Alberts *et al.*, *Molecular biology of the cell*, Garland, New York (1994).
 - [2] C. Peskin, G. M. Odell, G. F. Oster, *Biophys. J.* **65**, 316 (1993).
 - [3] A. Mogilner, G. Oster, *Biophys. J.* **71**, 3030 (1996).
 - [4] W. A. Eaton, J. Hofrichter, *Adv. Protein Chem.* **40**, 63 (1990).
 - [5] D. K. Fygenson, J. F. Marko, A. Libchaber, *Phys. Rev. Lett.* **79**, 4497 (1997).
 - [6] R. B. Dickinson, L. Caro, D. L. Purich, *Biophys. J.* **87**, 2838 (2004).
 - [7] A. Mogilner, B. Rubinstein, *Biophys. J.* **89**, 782 (2005).
 - [8] N.J. Burroughs, D. Marenduzzo, *J. Chem. Phys.* **123**, 174908 (2005).
 - [9] I. Derenyi, F. Julicher, J. Prost, *Phys. Rev. Lett.* **88**, 238101 (2002).
 - [10] D. R. Daniels, M. S. Turner, *J. Chem. Phys.* **121**, 7401 (2004).
 - [11] However a computation of the average membrane shape subject to the force in Fig. 3b (done as in A. R. Evans *et al.*, *Phys. Rev. E* **67**, 041907 (2003)) reveals that fiber and membrane do not intersect until well after the run-away transition.
 - [12] O. Medalia *et al.*, *Science* **298**, 1209 (2002).
 - [13] T. M. Svitkina *et al.*, *J. Cell. Biol.* **160**, 409 (2003); I. V. Maly, G. G. Borisy, *Proc. Natl. Acad. Sci. USA* **98**, 11324 (2001).
 - [14] D. Raucher, M. P. Scheetz, *Biophys. J.* **77**, 1992 (1999).
 - [15] M. R. Mejillano *et al.*, *Cell* **118**, 363 (2004); D. A. Schafer, *Nature* **430**, 734 (2004).
 - [16] A. Baumgartner, *Annu. Rev. Phys. Chem.* **35**, 419 (1984).